



A geophysical investigation of the urban-expanding area over the seismologically active Dahshour region, Egypt

Tarek Arafa-Hamed¹ · Hossam Marzouk^{1,2} · Samah Elbarbary¹ · Mohamed Abdel Zaher¹

Received: 29 August 2022 / Accepted: 6 June 2023 / Published online: 6 July 2023
© The Author(s) 2023

Abstract

Western Desert region between Cairo and Fayoum in Egypt is a geologically interesting area due to its active seismicity status and the continuous bidirectional urban expansions ongoing northward and southward growth. This work aims to develop a geological model of the region by combining magnetic intensity data (aeromagnetic) and potential field data (airborne gravity) with magnetotelluric (MT) data to offer decision-makers an additional evaluation tool for long-term future planning. Applying a number of filters to aerial gravity and magnetic data allowed us to calculate the subsurface density distribution and structure of the area between Cairo and Fayoum. In addition, the surface of the crust was imaged down to a depth of 6 km using a 3-D inversion of gravity data. Magnetotelluric data were gathered at eight locations over the NS-extended Cairo-Fayoum Road profile. MT data were inverted in 2-D to generate a resistivity model that defines the subsurface structure of the researched region. The subsurface geometry in the MT-derived resistivity model agrees with the results of airborne potential measurements, and no consideration was given to any faults that may have been undetected from the potential maps. Long-term seismological observations indicated that the likely active sources of earthquakes are limited to the recognized main faults and that the ongoing “1185 buildings” construction project did not and will not cause unanticipated seismicity. The paper concludes that urban growth is secure so long as the earthquake codes are rigorously considered while planning civil projects. The northern study region must be regularly monitored for induced seismicity. On the Cairo-Fayoum Road's western side, the middle sector of the study area is the safest place for future civil developments.

Keywords Aeromagnetic · Airborne gravity · Magnetotelluric · Electrical resistivity · Dahshour · Cairo-Fayoum · Egypt

Introduction

The significance of the research region (Fig. 1), situated north of the city of Fayoum in Egypt's western desert, stems from its intense seismicity and continuous northward and southerly urban growth. Moreover, the epicenter of the well-known Cairo earthquake of October 12, 1992, is located in the study area at Dahshour, 35 kms south of Cairo, and caused significant devastation in Cairo, Giza, and Fayoum cities.

Numerous investigations were conducted in the study region after the 1992 destructive earthquake. Even a minor earthquake, according to Celebi and Sharp (1993), may have widespread effects and result in a large number of casualties. Brimichi et al. (2011) investigated the subsurface tectonics of the region between Dahshour and El-Fayoum provinces utilizing magnetic survey and aeromagnetic datasets. They observed that the principal tectonic tendencies had orientations of EW, NE–SW, and NW–SE. Abdel Kader et al. (2013) demonstrated 3-D interpretations of magnetic and Bouguer anomaly maps in Fayoum, Cairo province region, Northern Western Desert of Egypt coupled with seismic data. They revealed that the basement rock in such a location has an uneven surface with faults going NNW, ENE, and NE. Khalil et al. (2014) investigated the underlying structure and tectonic setting in the Fayoum-Cairo area using aeromagnetic and seismic data. Their research reveals the presence of three major tectonic faults that run NE–SW, NW–SE, and E–W. Previously, Araffa et al. (2012, 2014) studied faults surrounding Cairo, particularly toward the

Edited by Prof. Bogdan Mihai Niculescu (ASSOCIATE EDITOR) / Prof. Gabriela Fernández Viejo (CO-EDITOR-IN-CHIEF).

✉ Tarek Arafa-Hamed
geointernational@netscape.net

¹ National Research Institute of Astronomy and Geophysics (NRIAG), Helwan, Cairo 11421, Egypt

² Present Address: Now at Institute of Geophysics, University of Münster, Corrensstr. 24, 48149 Münster, Germany

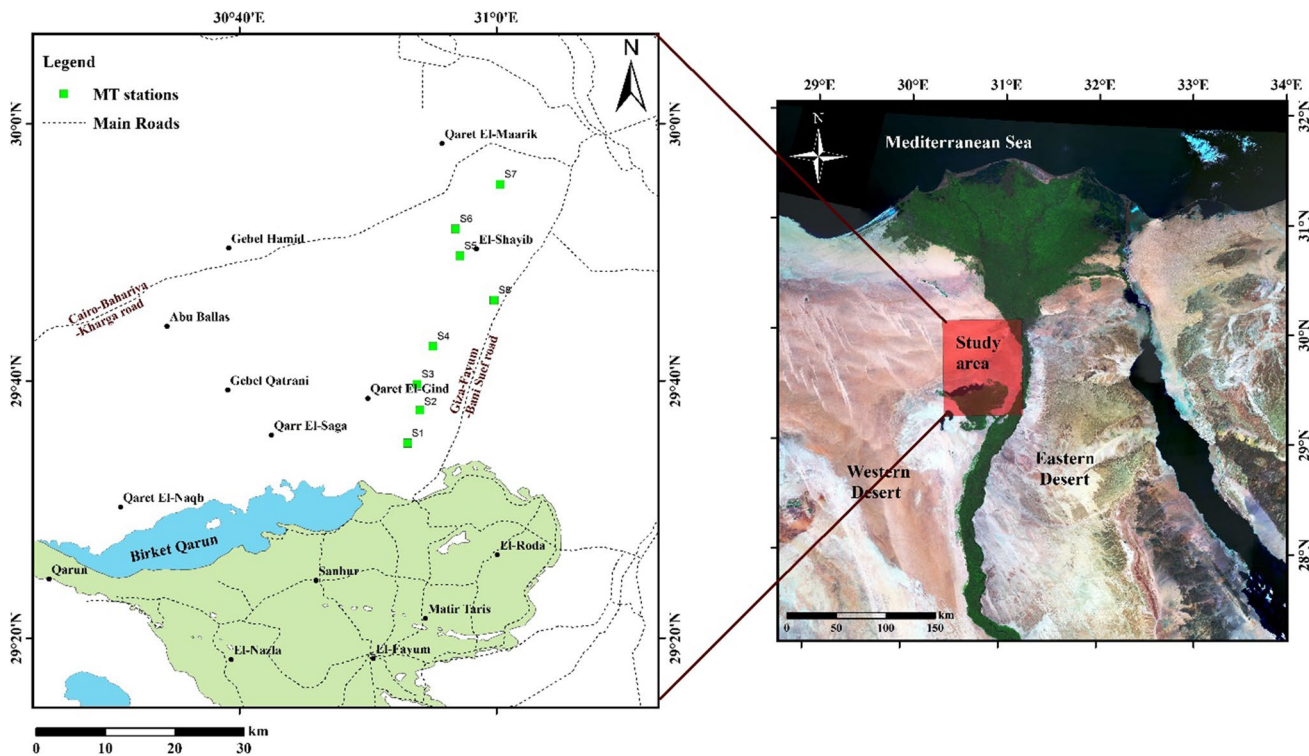


Fig. 1 Location map of the study area situated to the north of the Western Desert and to the south of Cairo. The green squares on the map refer to the locations of Magnetotelluric (MT) stations

northern end of the city, utilizing aeromagnetic, gravity, and seismological data.

The purpose of this research is to develop a comprehensive model of the region by defining the underlying structures and tectonics of the region along the Cairo-Fayoum Road utilizing the integration of aeromagnetic, aerogravity, as well as the newly acquired magnetotelluric (MT) data. Aeromagnetic data were subjected to the Euler deconvolution method as well as high and low-pass filters to get early estimations of the magnetic source locations and depths. While a map of the study area's basement relief was made using 3-D inversion of gravity data. Additionally, a reconnaissance MT survey was conducted along NS profile on Cairo-Fayoum Road. A conductivity model is created using MT data to show the subsurface structure underneath the research region from an electrical standpoint. The MT data and continually updated seismicity records from Egypt's national seismological network give an up-to-date assessment of the developing metropolitan region.

Geological and structure setting

The research area is between the cities of Cairo and Fayoum in the northern part of the Western Desert. It is bounded by latitudes $30^{\circ}6'$ and $29^{\circ}18'$ to the south, and longitudes

$30^{\circ}24'$ and $31^{\circ}10'$ to the east. The region is bordered on the south by Wadi El-Rayan and Qarun Lakes and on the east by the Nile Delta (Fig. 1).

According to Othman et al. (2016), the lack of Paleozoic and Jurassic rocks identifies the underlying sedimentary section, while the Upper Cretaceous sediments are represented by thick rock units arranged from top to the bottom as, Khoman Formation, Abu Roash Formation, and Bahariya Formation (Fig. 2). Some of these formations are seen on the surface in certain locations. The study area's surface geology spans various geological epochs, from the Lower Cretaceous to the Quaternary. The Quaternary deposits are represented by Nile silt, Sand dunes, playa, wadi, prenilite, and neonile deposits. Pliocene deposits are exposed to the north at Gebel Hamid. They are composed of Kom El-Shelul Formation which consists of sandstone beds and coquinal limestone. The Lower Miocene deposits are represented by Gebel Khashab Formation which is dark brown continental sandstone grading toward the west into Moghra Formation which is a continental to marine elastic sequence. The Oligocene sediments are represented by Gebel El-Ahmar Formation which is of continental-colored sands, quartzite, and gravel. The Qasr El-Sagha, Maadi, and Wadi Rayan formations reflect the Eocene age. The Oasr El-Sagha Formation is a coastal marine to continental elastic sequence including oyster beds intercalated with silt and clay stones.

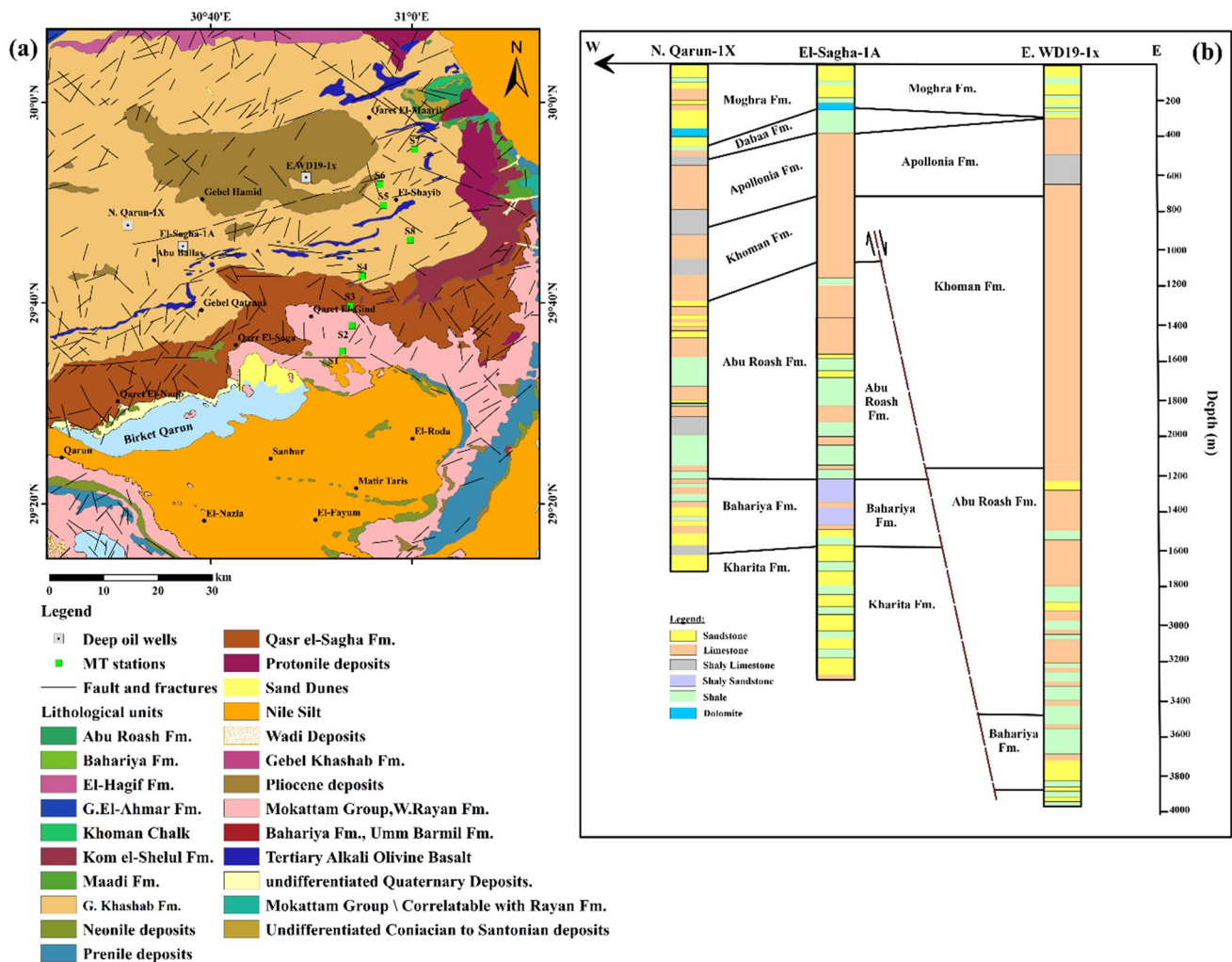


Fig. 2 a Surface geological map of the study area based on the Geological map of Egypt 1:500,000 NH 36 Beni Suef Conoco Coral [Egyptian General Petroleum Company (EGPC) 1987]; the black

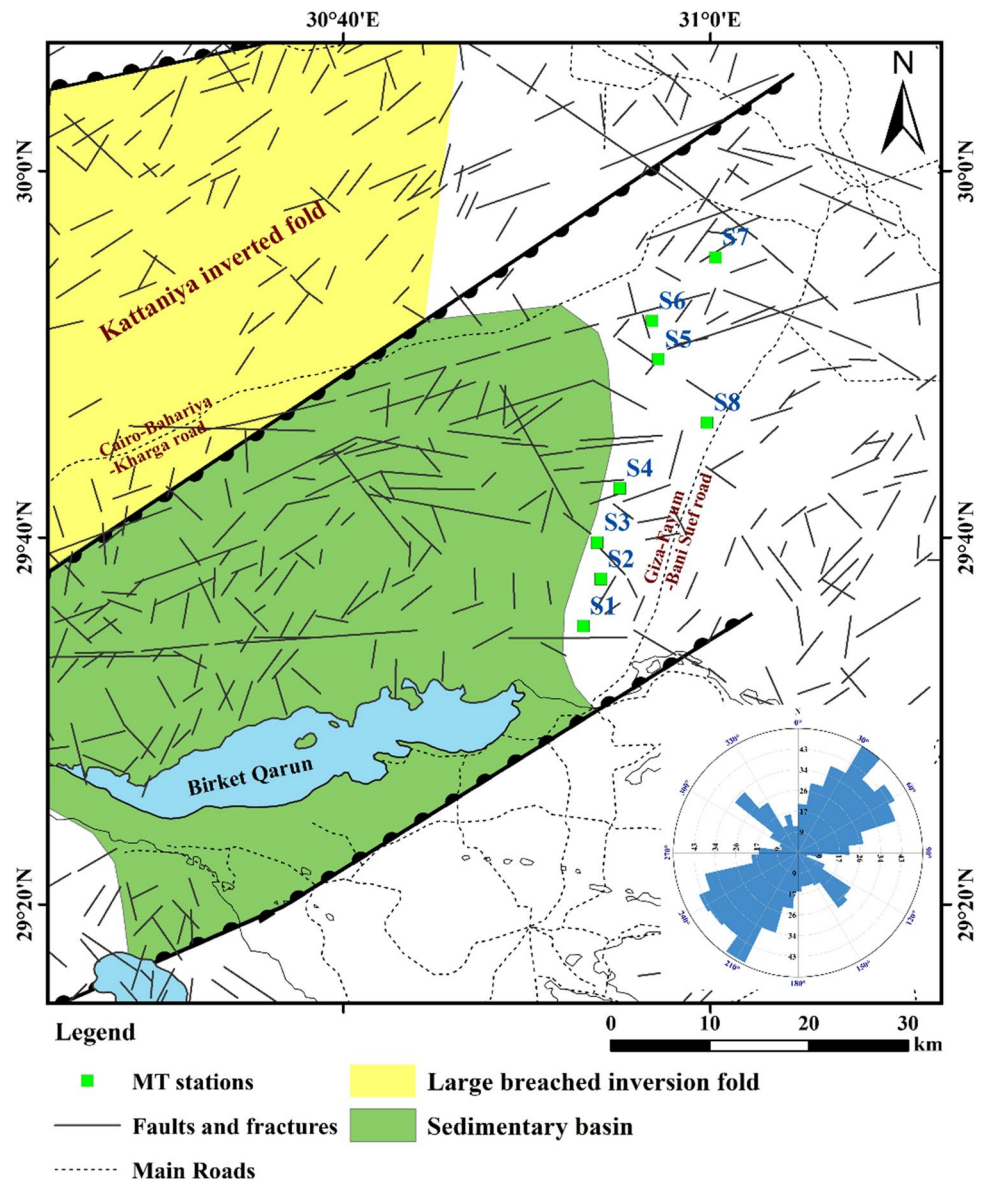
lines represent structural lines. b WE lithostratigraphic cross section through wells: North Qarun-1x, El-Sagha-1A, and E. WD19-1x in the study area, Egypt (modified after Hammad et al. 2010)

Maadi Formation is a shallow marine shale and limestone intercalated by shallow marine sandstone. In Wadi Rayan Formation, shallow marine limestone intercalated by shale and sandy shale. Khoman, Abu Roash, and Bahariya formations reflect the Upper Cretaceous period. Khoman Formation is a white massive of shallow marine chalk and chalky limestone. The majority of the Abu Roash Formation is composed of lutaceous calcarenite to calcarenite. The Bahariya Formation is made up of fluvial sandstone to siltstone at the bottom, and alternate layers of estuarine shale and sandstone at the top.

Structurally, the study region is distinguished by a basin and fold directed to the northeast that are associated with the Syrian Arc Structures (SASs). The fault-connected NE-to-ENE-dipping and double-dipping folds distinguish SASs (Khalil and Moustafa 1994; Ayyad and

Darwish 1996). Northern Kattaniya Basin is an elevated NE-trending anticline with a comparatively small north-western fore-limb and a large southeast back-limb due to Late Cretaceous tectonic inversion (Moustafa 2010). The main surface structural trends in the study area are ENE-WSW which follows the main trend of SAS and NE-SW which follows the Gulf of Aqaba-Levant system (Fig. 3). Both Figs. 2a, b and 3 show dense surface faults in addition to the major tectonics. These structures are suspicious while planning for urban constructions and hence are motivating for curious investigations. The Miocene, Oligocene, and Eocene strata cover the epicentral region of the 1992 earthquake (Said 1981). In the epicentral region, no surface tectonic lineaments have been seen. But several NW-SE and NE-SW faults have been observed close to the epicentral region. (Fig. 3).

Fig. 3 Structural and tectonic map of the study area [compiled after Egyptian General Petroleum Company (EGPC) 1987; Moustafa and Takenaka 2009; Bosworth et al. 2008]. Rose diagram (SE corner of the map) indicates that the main structural trends NE–SW and ENE–WSW. The wide spreading fault-structures in the area trigger repeated and updated investigations along with civil works



Geophysical data processing and analyses

Several geophysical datasets obtained from a variety of sources have been integrated in order to accomplish the goal of evaluating the underlying structural settings of the study area. The seismicity, aeromagnetic, aerogravity, and MT surveys are all included in these data.

Seismicity data

This study's location is well acknowledged to be tectonically active. The epicenter of the well-remembered Cairo earthquake of October 12, 1992, was at Dahshour, 35 km south of Cairo. Despite having a modest magnitude of 5.9, the earthquake was very damaging, resulting in 561 fatalities and considerable damage to thousands of historic

structures in Cairo, Giza, and Fayoum (Mossaad 1996). Consequently, regularly updated information concerning the seismicity of Dahshour and its environs must be taken into account when planning any urban growth.

The Egyptian National Seismic Network (ENSN) is where seismicological data were obtained and retrieved. It retains continuous seismicity data records by keeping a database with continuous seismicity data recordings for the whole country of Egypt. Figure 4 depicts the distribution of earthquake epicenters in the study area from 1997 to 2018. The shown epicenters are categorized into six depth categories from the surface to a depth of 34 km. The majority of seismic activity, especially deep earthquakes (30 km), is focused in the middle of the eastern portion of the study region.

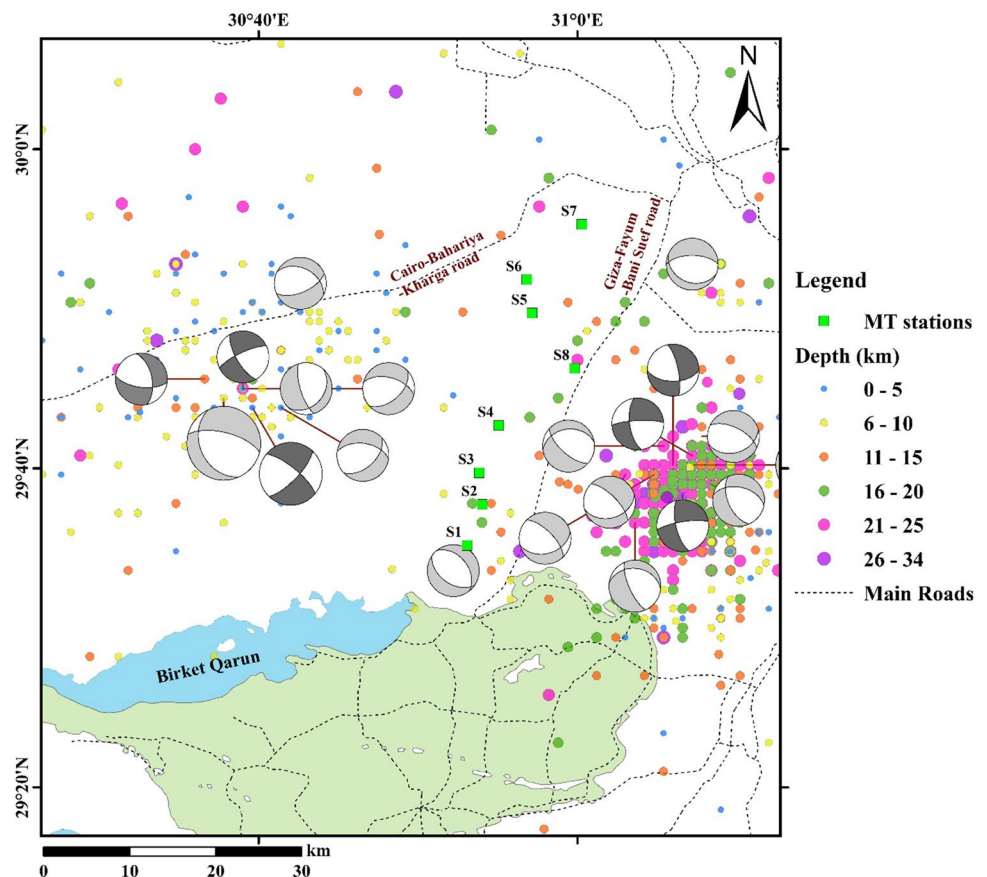
Furthermore, a number of shallower earthquakes (0–10 km) were recorded on each side of the Cairo-Bahariya-Kharga route in the west-central region. In the west-central part of the region, however, many shallower (0–10 km) earthquakes occurred on both sides of the Cairo-Bahariya-Kharga road. This may indicate that some of the widely dispersed small-scale faults shown in Figs. 2 and 3 are active or might be triggered by human activities like intensive housing cultivation of arid areas or even mining of basalts and phosphates. The areal distribution of the shallow epicenters suggests that the local faults toward the southern end of the developing metropolis (near the northern MT stations) are neither active nor have been triggered prior to 2019 (Fig. 4). Abou Elenean (1997) categorized the Dahshour region as a seismogenic zone based on an examination of the epicentral distribution, seismicity intensity, and similarity of focal processes. There were three significant seismic events that occurred east of the Dahshour region inside the Suez-Cairo shear zone (October 30, 2007, Local magnitude scale (ML) = 3.7; July 07, 2005, ML = 4.2; June 29, 2000, ML = 4) (Abou Elenean et al. 2010). All of these phenomena are caused by typical faults with strike-slip motions.

Aeromagnetic data

The aeromagnetic data come from Getech's study that was compiled as part of “African Magnetic Mapping Project” (AMMP) (Green et al. 1992; Getech 1992) and presented as Total Magnetic Intensity (TMI) grid that is 1 km in size. The level flying mode was used during the survey, and the flight lines were orientated in an E-W direction. Nearly 3 km separated each flight line, and the altitude of the aircraft was 450 m. –190 nT to 135 nT are the overall magnetic intensity anomalies (Fig. 5a). The predominant magnetic anomaly directions are east–west. Using magnetic separation and Euler deconvolution, the TMI is utilized to investigate regional and residual subsurface faults. An attempt was made to differentiate between the regional magnetic field, which stems from deep-seated sources, and the residual field, which is linked to shallower structures. In the current investigation, regional-residual components were separated using the power spectrum approach being a predominant method in enhancing magnetic anomalies (Hinze et al. 2010) (Fig. 5b).

The regional magnetic map (Fig. 6a) has the same general look as the TMI map (Fig. 5), suggesting that shallow structures do not obscure the anomalies of the deep-seated structures. The values of the regional magnetic anomaly vary

Fig. 4 Spatial distribution and depth-classification of earthquake epicenters occurred in the study area during the epoch from 1990 to 2019. The destructive Earthquake of 1992 belongs to the cluster of deep epicenters obvious on the eastern side of the province. The data are provided by the Egyptian National Seismic Network (ENSN). Shallow earthquakes occur on both sides of the Cairo-Bahariya-Kharga road. Locations of magnetotelluric stations are indicated by small green rectangles. The ongoing urban expansion reached the area of the northern magnetotelluric stations



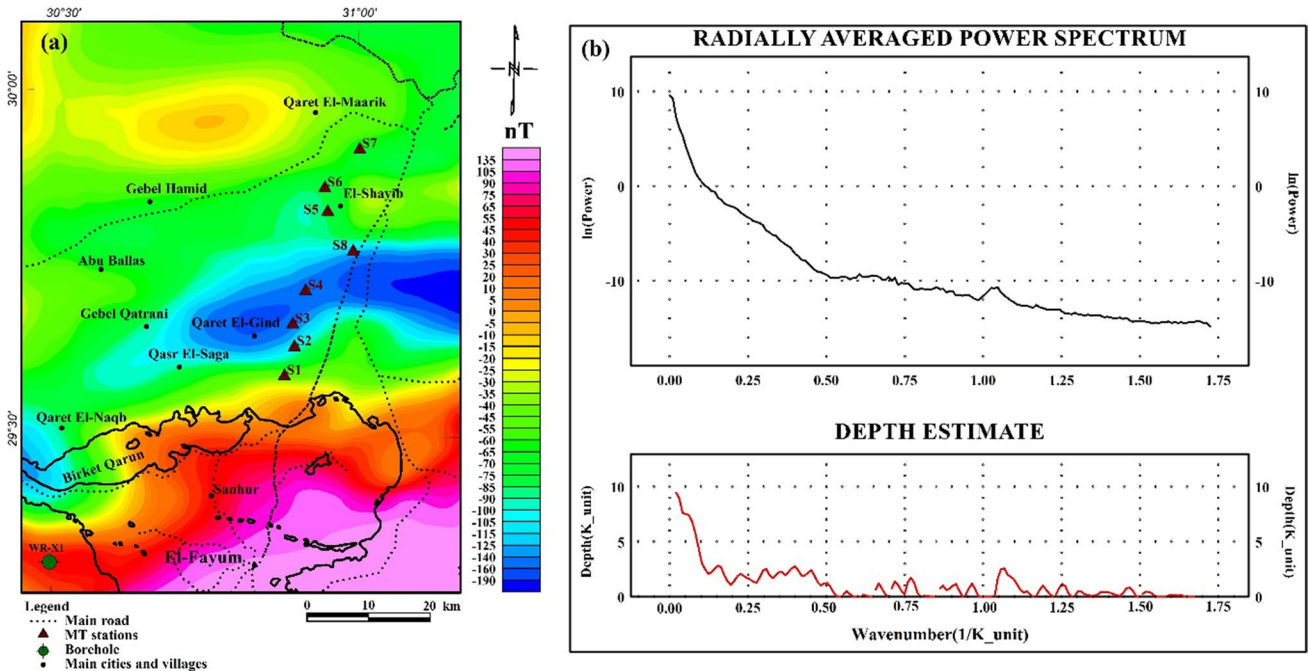


Fig. 5 a Total magnetic intensity (TMI) map of the study area extracted from Getech's compilation study (Getech 1992; Green et al. 1992). b The radially averaged power spectrum of the magnetic map

between -156 and 178 nT. The map's structural features reveal that three distinct major trends are present in the area: NE–SW, WNW–ESE, and ENE–WSW. Deformation lineaments may also be seen in the zones when there are large differences in anomalies between low and high levels. The residual magnetic contour maps (Fig. 6b) are used to outline the research area's shallow-seated structural features (Fig. 6c). ENE–WSW (Trend of the Syrian arc system), WNW–ESE, NNE–SSW, and E–W trends are the four primary trends of the subsurface faults that have been extracted.

Furthermore, the residual magnetic data were deconvolved using the 3-D Euler method. It is a method used to estimate the depth of a source that generates a magnetic signature in an area (Ghosh 2016). It employs the field's derivatives in X , Y , and Z dimensions to estimate the position and depth of different targets include dyke/sill, contact, sphere, and cylinder using a particular Structural Index (SI) (Reid and Thurston 2014). SI measures the rate of field degradation as distance from the source increases. In the Standard Euler approach, the homogeneity equation of Euler (Thompson 1982) is used to link anomaly sources' locations to the magnetic field and its gradient components.

$$(x - x_0) \frac{\partial T}{\partial x} + (y - y_0) \frac{\partial T}{\partial y} + (z - z_0) \frac{\partial T}{\partial z} = N(B - T), \quad (1)$$

where B is the magnitude of the regional total field and (x_0, y_0, z_0) is the position of a magnetic source whose total field T is measured at (x, y, z) .

The 3-D Euler deconvolution approach entails establishing an acceptable SI and solve the equation for the optimal B and x_0, y_0, z_0 utilizing least-squares inversion across a square window size (2.9 km) comprised an integer number of grid cells in the dataset. Euler deconvolution method is used with Structural Index (SI)=0. The SI value of 0 (Prism geometry) is reported to be suitable for areas with faults and basement relief (Melo and Barbosa 2018). Euler's solutions suggest source depths between 500 and 4000 m, the locations of these solutions correspond to those calculated from the residual magnetic filter. The trends at these locations include ENE–WSW (trend of the Syrian arc system), WNW–ESE, and E–W (Fig. 6d).

Airborne gravity data

The gravity data used in this investigation were received from the GETECH Group PIC as part of the African Gravity Project (AGP) (Fairhead et al. 1988). An elevation gradient of 0.3086 mGal/m is utilized for the free air adjustment and a reduction density of 2670 kg/m³ for the Bouguer correction on gravity data (Getech 1992). The study area's northwest is shown to have a positive anomaly on the Bouguer anomaly map, which spans the range of -31 to 4 mGal and progressively diminishes toward the

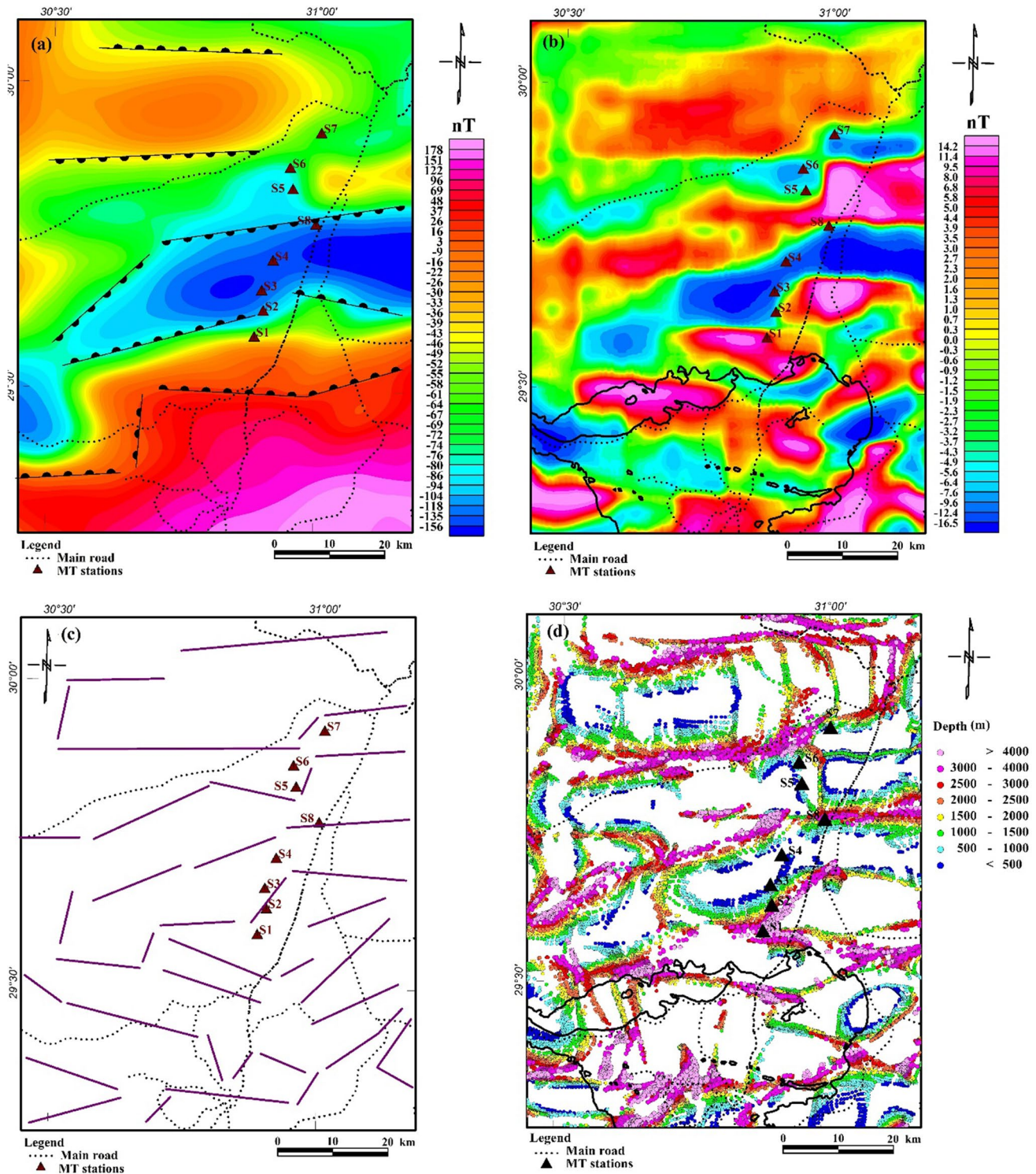
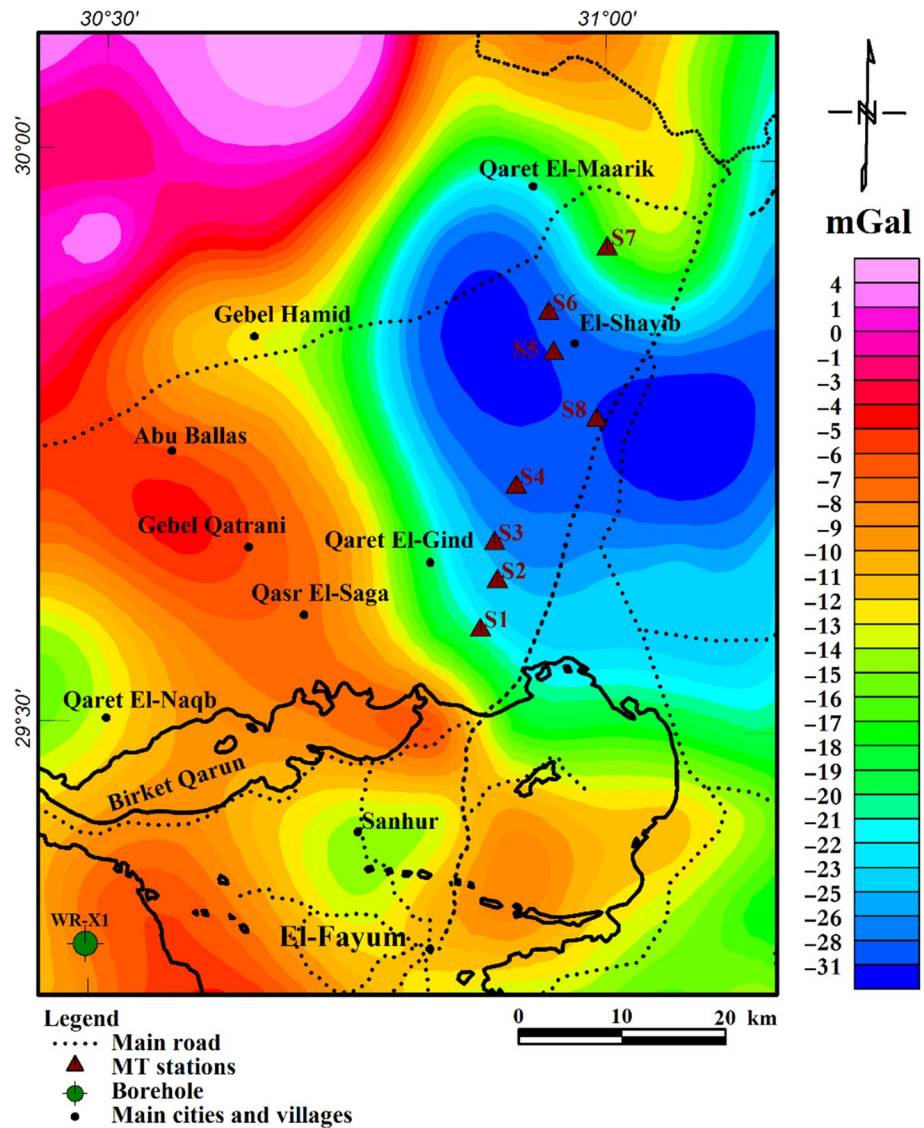


Fig. 6 **a** The low-pass filtered regional magnetic map, **b** the high-pass filtered residual magnetic map, **c** the shallow-seated structural elements extracted from the residual magnetic map, **d** the Euler deconvolution solution using structural Index (SI)=0

east, suggesting an increase in sedimentary rock thickness toward the east (Fig. 7). Gravity data are utilized to build a 3-D density model for the research area.

Bouguer data were inverted in 3-D to delineate the depths of the higher density basement rock below the study area. The inversion is performed using the GRABLOX-1.6

Fig. 7 Bouguer anomaly map of the study area as provided from the African Gravity Project (AGP) (Getech 1992). The free air correction uses an altitude (elevation) gradient of 0.3086 mGal/m, whereas the Bouguer correction uses a 2670 kg/m³ density



software, which computes the Bouguer anomaly of a 3-D block model and optimizes the block thickness using singular value decomposition (SVD) in order to minimize the misfit between observed and estimated gravity. BLOXER-1.5 program is also used for interactive visualization of the 3-D block model (Pirttijärvi 2004). The starting model is oriented North–south, which spans 120 km north to south and 100 km east to west using 154 and 148 grid units, respectively. The buffering effect was accomplished by including three additional blocks as margins that had no impact on the computational area. Consequently, the block model has (45,584) small blocks, including the novel discretization (XYZ) of (154 × 148 × 2) blocks, with a default block size of (685 × 776.2 × 2500 m³) (Fig. 8). The initial model's apex was lie on a flat plane at sea level.

The model uses crystalline foundation rock with a density of 2670 kg/m³ and sedimentary rocks with a density of

2400 kg/m³. Because we relied primarily on two layers, we could only optimize the height of each individual block by using the inversion method in order to bring the observed gravity data more in line with the predicted values. Every minor block has its own unique setting for the fixed density. Height inversion is a technique that allows for an investigation of the fluctuating thickness of the sedimentary layer by using a constant density contrast. The Occam's razor method to optimization uses the concept of least complication to reduce the amount of model roughness and data misfit.

Deep well data on the average densities of the major lithologic units in northern Western Desert of Egypt were used to compute sedimentary rock density (Abu El-Ata & Abd El-Nabi 1985; Abdel Zaher et al. 2018). An optimized regional field is created before performing an inversion, such that only masses located inside the model's volume will have a gravitational influence on the inversion.

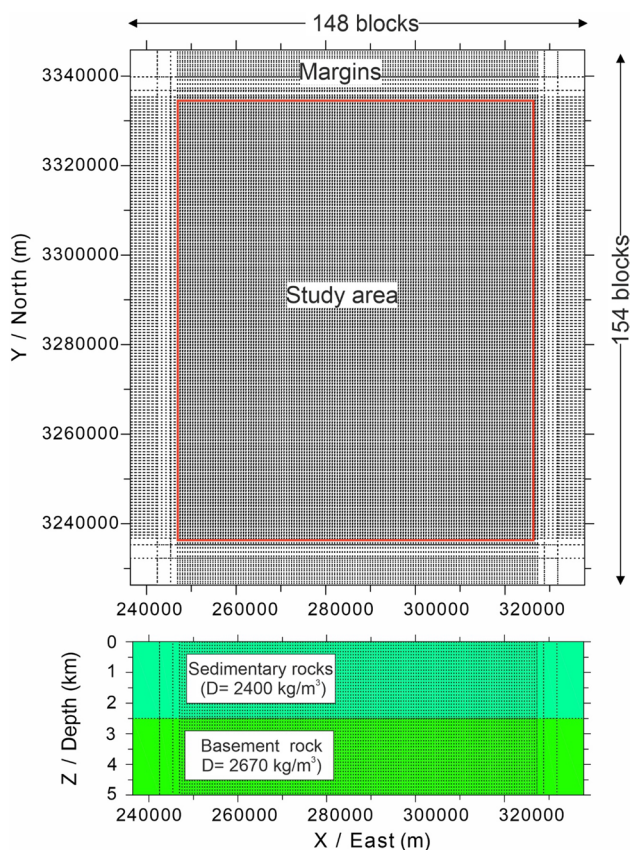


Fig. 8 Plane view of the grid blocks for the overall 3-D gravity model of the study area and EW slice shows the two subsurface layers used in the model (sedimentary rocks with density 2.4 gm/cm^3 and basement rocks with density 2.67 gm/cm^3). Coordinates are in meters using UTM 36N projection

Figure 9 illustrates the outcomes of the 3-D gravity inversion. Comparing the original Bouguer gravity map (Fig. 9a) with the one derived for the crustal model (Fig. 9b) reveals a decent fit. As seen on the misfit map in Fig. 9c, the majority of error values are positioned extremely near to zero mGal, and the gravity model's Root Mean Square (RMS) value is 1.6×10^{-3} . From the output of the 3-D gravity inversion, the depth to the deep crystalline rock that corresponds with the sedimentary layer's full-scale thickness was determined and plotted (Fig. 9d). The resulting map indicates that the depths to the basement surface vary between 300 and 4200 m. The shallowest depths are found toward the south of the Fayoum depression. The NW–SE trend of the deepest basement depth ($> 4200 \text{ m}$) divides two main basins in the southern and northern regions. The generated section (Fig. 10) demonstrates substantial agreement between the genuine basement depth (2100 m) from oil well (WR-X1) in the southwestern portion of the research region (see Fig. 9 for well location) and the depth calculated using 3-D block model gravity data.

Magnetotelluric data

Magnetotelluric (MT) is a geophysical technique that uses the earth's intrinsic electromagnetic field as a passive source to obtain electrical resistivity parameters from shallow depths all the way down to the deeper mantle, which is considered a passive source by MT (Simpson and Bahr 2005). MT data are comprised of electric and magnetic fields recorded at the Earth's surface. An impedance tensor (Z) that is frequency dependent and susceptible to the Earth's underlying electrical conductors connects these two fields

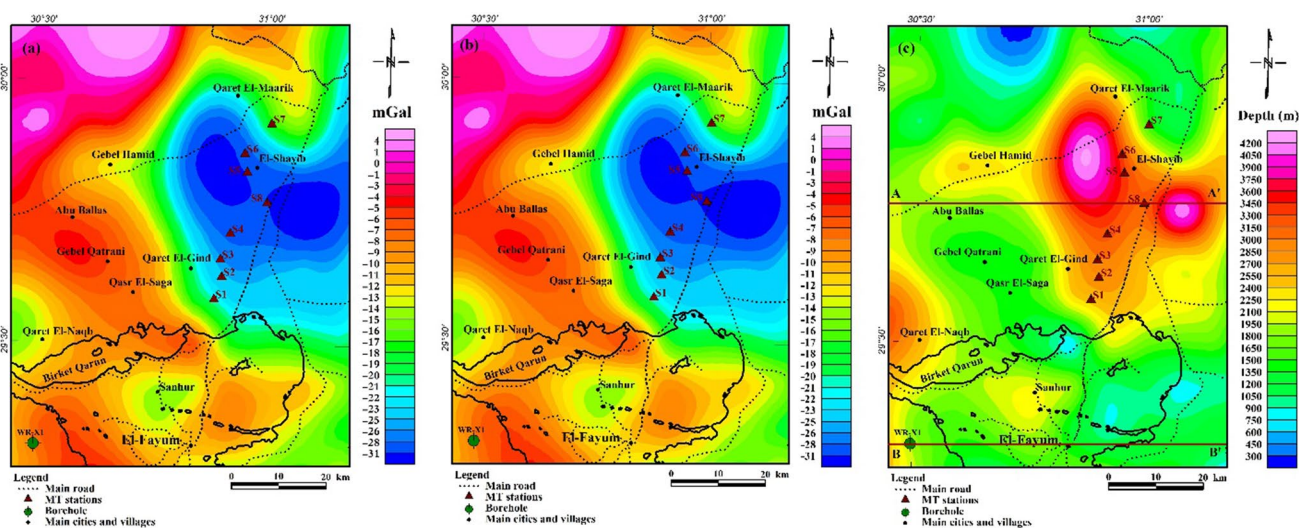


Fig. 9 Resultant maps from the 3-D gravity modeling. **a** The observed gravity anomaly, **b** the computed gravity anomaly, and **c** basement relief map derived from the 3-D density modeling with the location of the two depth slices (AA' and BB') presented in Fig. 10

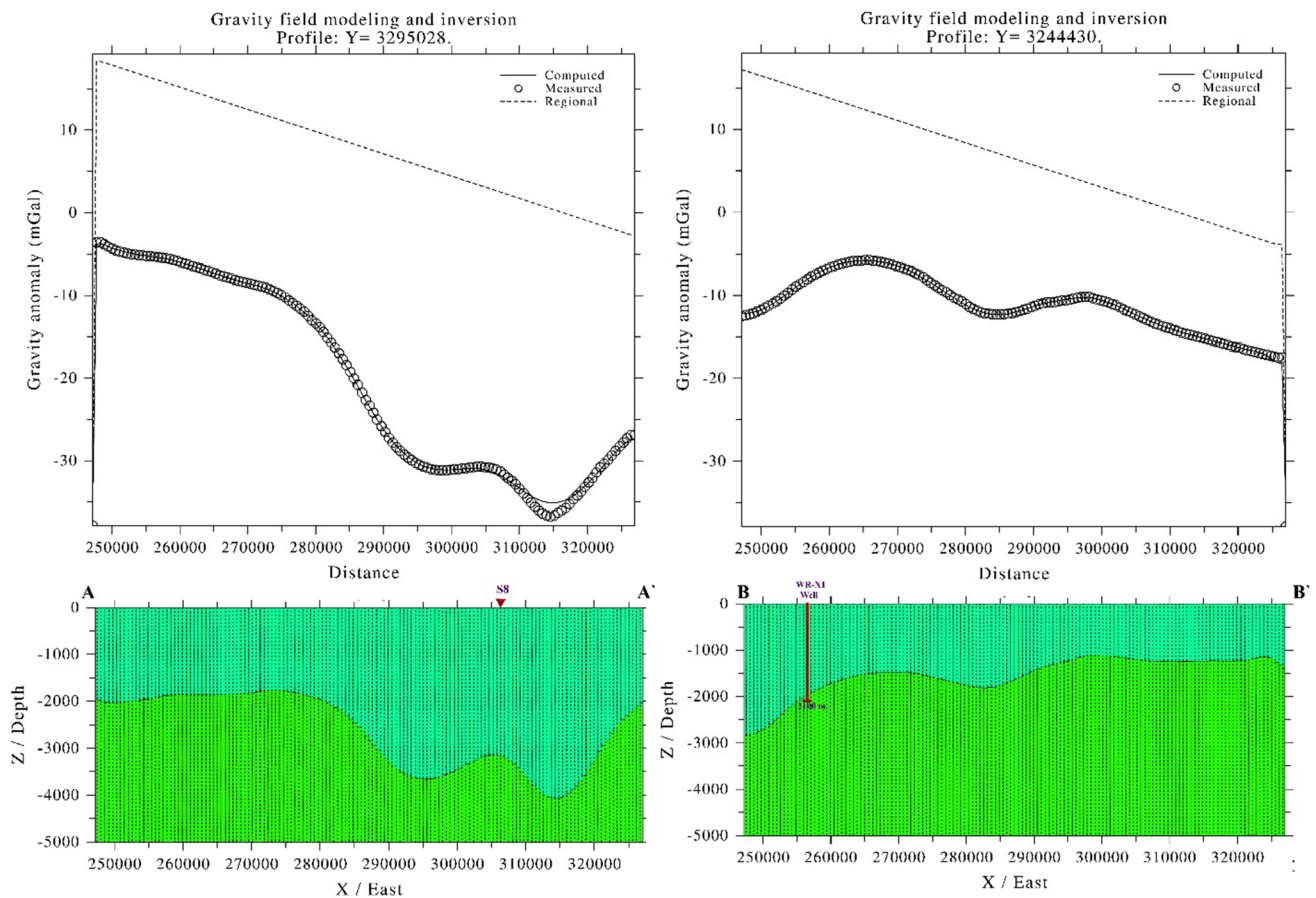


Fig. 10 EW density models from the 3-D gravity inversion illustrate the results from the fitting of the observed (circles) and calculated (line) gravity data. To the left (AA'), the density model of the slice crossing the MT station number 8, to the right (BB'), EW density

model of the slice passing through WR-X1 well shows that the depth of the basement in the well (2100 m) nearly matches that obtained by modelling. The locations of the profiles (AA' and BB') are presented in Fig. 9c

(Chave and Jones 2012). In recent years, the MT technique has advanced greatly and is now employed in hydrocarbon exploration in areas where seismic exploration is uphill. The MT approach has been frequently employed in geothermal research in recent decades (for instance, Di Paolo et al. 2020; Hersir et al. 2020), in subsurface structural imaging (i.e. Comeau et al. 2020), and in imaging the lithospheric structures (i.e. Käüfl et al. 2020).

The electrical conductivity of rocks is typically a good indicator of major tectonic features, as is their compositional change and deformation. Thus, including resistivity models in the research region might benefit in comprehending the non-uniqueness of crustal structure as identified by seismic and potential field data.

Data acquisition and analysis

The MT data were collected over a 40-km profile parallel to the Cairo-Fayoum Road at 8 MT stations spaced at 5-km intervals. Each location was chosen to be in close

proximity to no electrical facilities, such as railway traction, power plants, or human populations. Additionally, the locations are positioned away from significant bodies of water and, ideally, on 100 × 100 m flat plains. According to the positions of the MT stations (Fig. 1), the current research area is regarded as optimal for the placement of MT stations.

Metronix ADU-07e was used for data logging provided by NRIAG in Egypt and three magnetic induction coils (Metronix MFS-06e) have been utilized for recording the magnetic field in the three orthogonal directions. The magnetic coils are characterized by a wide range of frequencies (0.0001 Hz–10 kHz). With 100 m dipole length, 2 sets of non-polarizable electrodes of Pb–PbCl were used to measure the telluric currents in orthogonal north and east directions at each station. The electrodes were buried to protect them from dehydration, human or animal interference, and temperature fluctuations. While induction coils were employed to record the components of the magnetic field, they were buried at a depth of 10 to 30 cm to limit the impacts of

temperature change, microseismic tremors, and wind noise, as shown in the schematic sketch of Fig. 11.

Dimensionality analysis of the MT response was done utilizing phase tensors and the ellipticity criterion (Caldwell et al. 2004; Becken & Burkhardt 2004). An ellipse is used to graphically illustrate the phase tensor. The tensors will be represented as circles for 1-D and as ellipses for 2-D or 3-D subsurface resistivity. By evaluating the degree of asymmetry of the phase, the skew angle (β) may also be utilized as a dimensionality evaluation tool. Skew angles of zero are required for a purely 2-D resistivity structure; however, large values of skew ($> 6^\circ$) suggest strong 3-D impacts (Booker 2014).

As seen in Fig. 12, the skew angles of the phase tensor ellipses are reflected in the colors of the ellipses, which are shown in MT response pseudosections throughout the profile. The phase ellipses are almost circular and have modest ellipticity at all stations for most times in the dataset, indicating that a 2-D model is viable. The mask used before modeling had a skew value greater than 5 degrees because certain places showed distortion for extended periods of time.

2-D modeling of MT data

A 2-D model of subsurface resistivity was generated from the MT data (Fig. 13) utilizing MARE2DEM algorithm (Modeling with Adaptively Refined Elements for 2-D Electromagnetics). It is a parallel adaptive finite element code for 2-D forward and inverse modeling for electromagnetics. The forward solution in MARE2DEM uses fully automatic goal-oriented adaptive finite elements while the nonlinear inversion uses a fast parallel implementation of Occam's method, a regularized Gauss–Newton minimization technique, that automatically generates and modifies unstructured triangular components (Key 2016).

The MT data were flipped to align with the estimated geoelectric striking direction (Fig. 12b) and then projected onto a perpendicular straight profile. A $100 \Omega\text{m}$ half-space mesh was utilized as an initial model, omitting long-term data with skew distortion. In addition to a 5 percent apparent resistivity error floor and a 1 degree phase error floor, An τ -value of 5 was selected as the ideal control value to balance model roughness and model-data mismatch. With a total root mean

Fig. 11 Schematic sketch of standard Magnetotelluric station setup with the Metronix ADU-07e datalogger in the center and four sets of non-polarizable electrodes buried 30 cm deep alongside with two magnetic coils buried horizontally and one coil which is buried vertically and well leveled

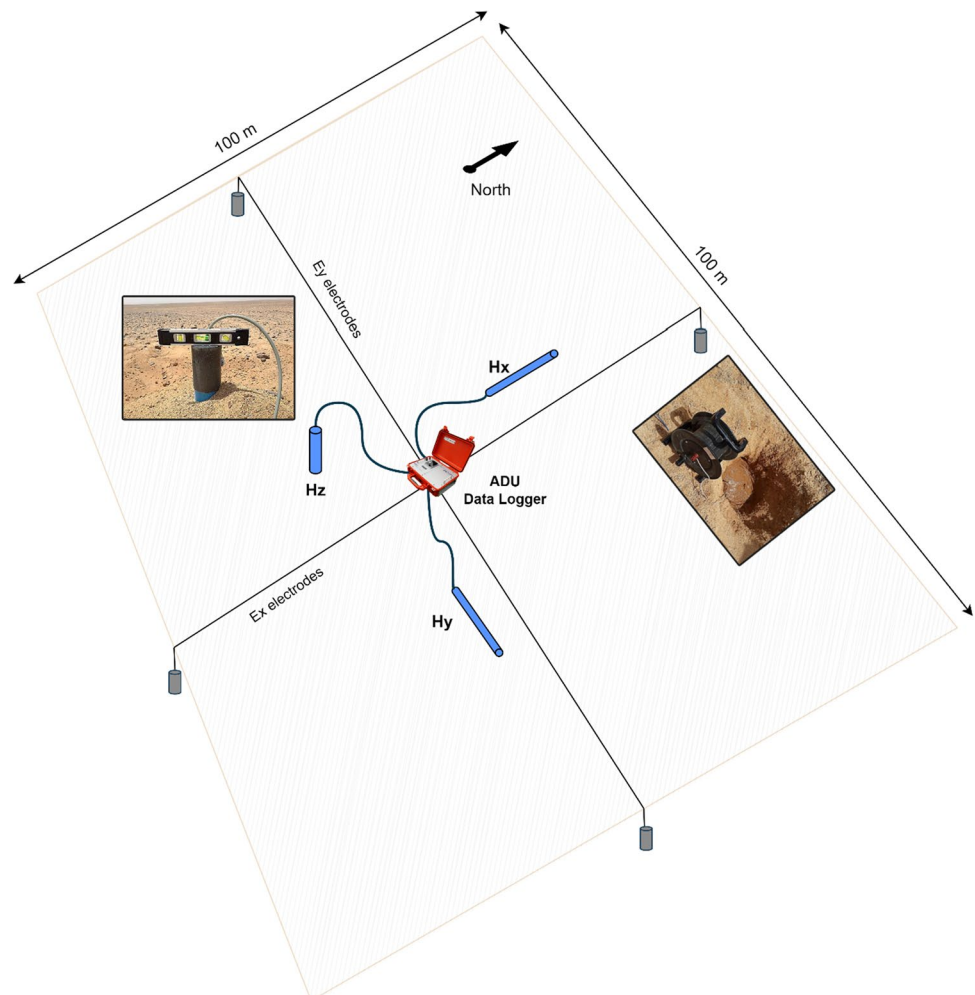


Fig. 12 Phase tensor and geo-electric strike analysis generated by MTPy (Kirkby et al. 2019; Krieger and Peacock 2014). **a** Phase tensor ellipses for all periods and all sites plotted along the acquired profile and colored with their skew values. The most of the phase tensors are characterized by circular shape and low skew values, which indicates 1-D or 2-D geo-electric structure. **b, c** Rose diagram of the geo-electric strike direction and the phase tensors azimuth, respectively, along the profile for all the periods. The preferred direction is estimated to be N62°E, which matches the geological strikes estimated at Fig. 3

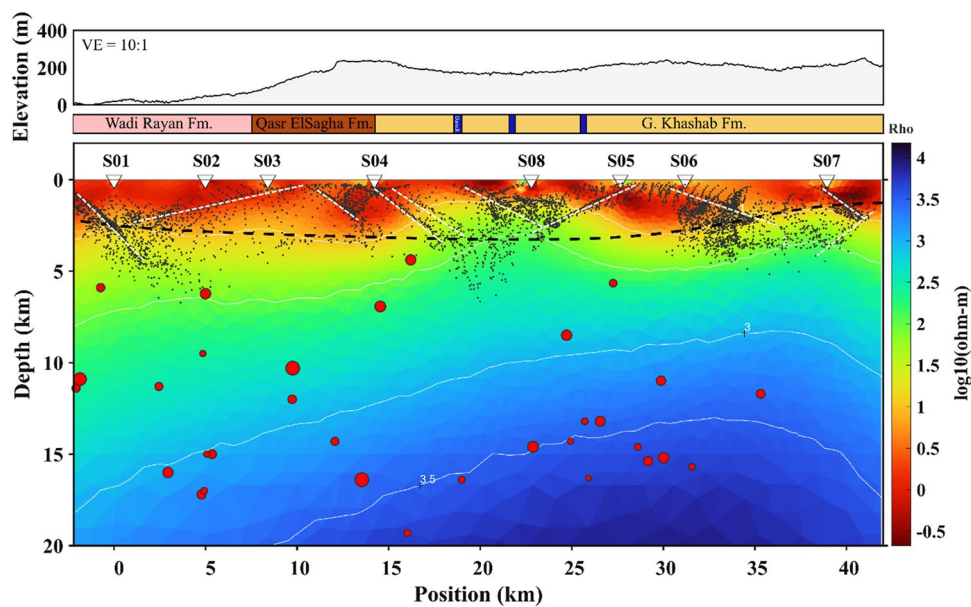
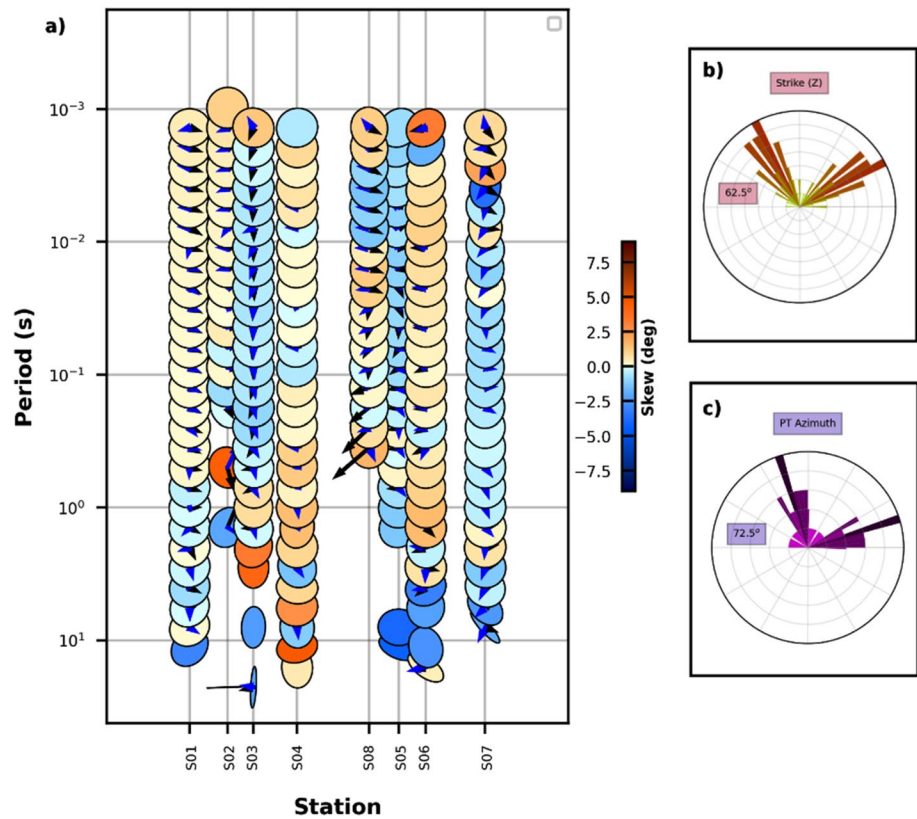


Fig. 13 The preferred 2-D resistivity model, obtained from inversion of 8 MT sites (location in Fig. 1), with white solid lines representing resistivity contour lines. The topography was included in the model and is shown in the upper panel with a vertical exaggeration (VE) of 10:1. Geology along the profile extracted from (Fig. 2) and is shown in the second panel. Gray dots represent the Euler solution calculated

from magnetic data alongside with its associated faults in dashed white lines (Fig. 6). The depth of basement obtained from gravity inversion (Fig. 9) is in black dashed line. Distribution of nearby epicenters (in red dots) (Fig. 4), with smallest radius representing 2.9 ML and the biggest radius corresponding to 5.9 ML

square misfit (RMS) 1.3, the inversion technique reached a smooth convergence after 13 iterations. The outputs were then inverted again using phase two of the algorithm, which seeks to decrease roughness norms. The smooth model was developed after two iterations and is the favored model.

At the surface, Fayoum area is surrounded by the Late Cretaceous-Eocene El-Gindi basin and Jurassic-Cretaceous sediments of Kattaniya province (Fig. 3). In the MT model, the near-surface conductive layer reflects the sedimentary basin with a level of accuracy that is satisfactory regarding resistivity and thickness (Fig. 5). Estimates of sedimentary basins in the region are consistent with the resistivity readings, which are in the range of 1–20 Ωm (Afife et al. 2018, Hamad et al. 2010).

The resultant preferred model exhibits strong spatial correlations between gravity and magnetic anomalies and enhances the interpretation of basement and structure. Northward and southward of the profile, the sedimentary succession and the depth to basement are in agreement with the results from magnetic and gravity datasets. On the other hand, in the middle part of the profile where the tertiary basaltic lavas are exposed to the surface, the magnetotelluric method reveal more details than the other potential methods. The thickness of these basaltic lavas ranges from 2 to 25 m and capped the upper Qatrani escarpment. It was extruded in the late Oligocene from fissures caused by a tensional tectonic activity accompanied by northwest-trending normal faults in the northern portions of Egypt's Eastern and Western Deserts (Rittmann 1954).

The MT results show the conductivity signature of such extrusion, in which the thickness of the conductive sedimentary cover is decreased toward these basaltic sheets and increase outward from it that could indicate that the local source vents are probably buried northern or northeastern of the Fayoum Depression (Bown and Kraus 1988).

Data integration and conclusions

Integration of data from many sources and geophysical techniques enables to comprehend the underlying structural configuration of the study area. The extension of civil structures as part of the “1185 Buildings” project near the southernmost tip of Cairo prompted a current examination of the Dahshour-Fayoum area. Figure 13 depicts the projection of seismological event epicenters on the resultant geoelectric inverted section, as well as the depths to basement constructed from the 3-D inverted gravity data, and faults

estimated from the 3-D Euler deconvolution of aeromagnetic data.

Implementation the findings from a 2-D MT model and a 3-D gravity inversion is used to infer the subsurface structures, represented by outline of basement surface faults in the geological sequence. Continuous to a depth of 20 km, the 2-D resistivity model showed an image of underlying sedimentary cover down to the Pre-Cambrian foundation rock. The 3-D gravity inversion was capable to identify the relief of the crystalline basement rocks, which corresponds to the top-surface of a highly resistive layer in the MT section.

The Pre-Cambrian basement rock, which appears as a deep high resistivity layer ($> 1000 \Omega\text{-m}$), has depths varying from 1.2 km in north up to 3 km to the south. In addition, the elevation of the basement rock to the north of the section is characterized by an accumulation of several seismic events, and it is possible that this uplift is connected to the subsurface extension of the Dahshour fault. Away from these consistent results about existing structures of the province, the study showed no hidden structures that might be source of unexpected hazard. The distribution of shallow earthquakes confirms that no induced seismicity is generated during the last 20 years. The epicenters are not biased in their spatial characteristics to the new buildings in any form.

Satellite images show the large urban sprawl of the recent period in the direction of seismically active locations (Fig. 14), which raises the alarm about the extent to which safety standards are adhered to during the construction of these urban communities. Although one has little control over the seismic hazard, the most essential elements in saving lives and decreasing earthquake losses can be enhanced by curious considerations.

Within the study area, precautions need to be taken into account during the construction of new communities based on adoption of modern building codes enforcement (earthquakes). This is necessary in order to avoid experiencing similar influences to those that were caused by the earthquake disaster that occurred in 1992, which had its epicenter at Dahshour. Furthermore, induced seismicity must be continuously monitored by local stations specially after settling the population in the new buildings and the expected human impact on widely existing shallow faults in the region (Tracy and Javernick-Will 2020). It is also recommended to avoid expanding on the easternmost portion of the study region as well as the western side around the Cairo-Wahat-Kharag while planning for near future settlements. The middle of the area, along Cairo-Fayoum Road's westbound side, remains the safest sector and is large enough for expansions during the next 30 years.

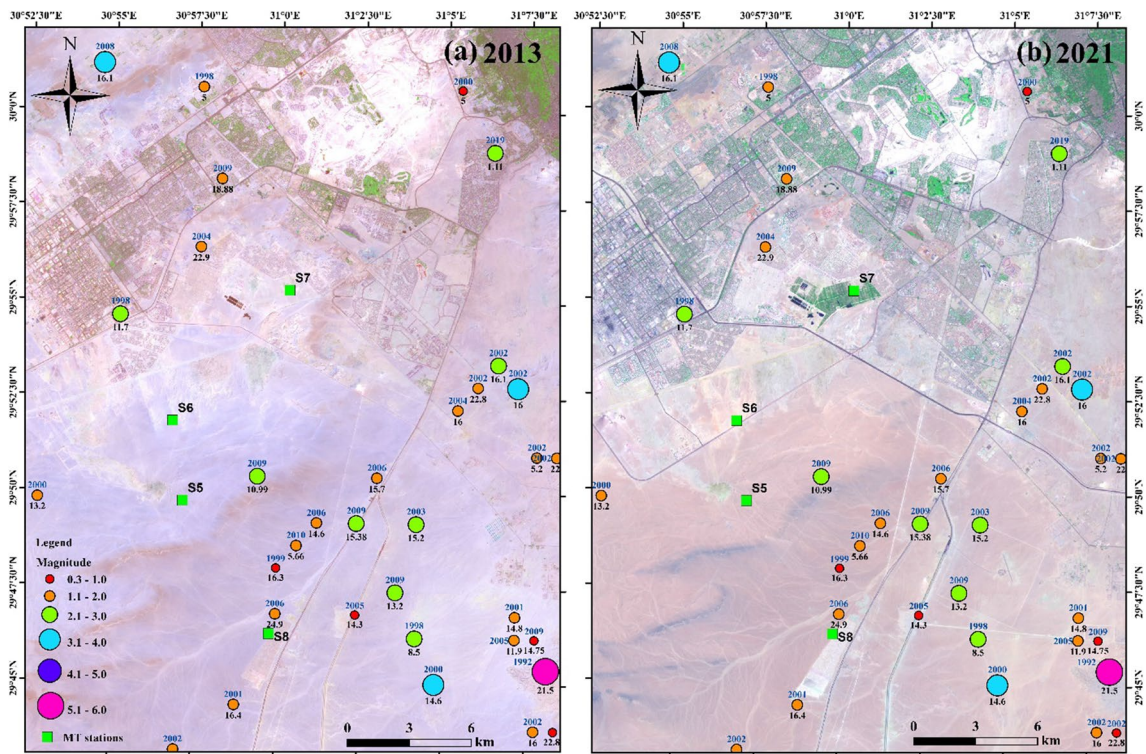


Fig. 14 Landsat 8 images of the study area captured in **a** 2013 and later in **b** 2021 demonstrate the development that has taken place in the metropolitan areas

Funding Open access funding provided by The Science, Technology & Innovation Funding Authority (STDF) in cooperation with The Egyptian Knowledge Bank (EKB).

Declarations

Conflict of interest On behalf of all authors, the corresponding author states that there is no conflict of interest.

Open Access This article is licensed under a Creative Commons Attribution 4.0 International License, which permits use, sharing, adaptation, distribution and reproduction in any medium or format, as long as you give appropriate credit to the original author(s) and the source, provide a link to the Creative Commons licence, and indicate if changes were made. The images or other third party material in this article are included in the article's Creative Commons licence, unless indicated otherwise in a credit line to the material. If material is not included in the article's Creative Commons licence and your intended use is not permitted by statutory regulation or exceeds the permitted use, you will need to obtain permission directly from the copyright holder. To view a copy of this licence, visit <http://creativecommons.org/licenses/by/4.0/>.

References

- Abdel Kader AK, Kordik P, Khalil A, Mekkawi M, El-Bohoty M, Rabeh T, Refai MK, El-Mahdy M (2013) Interpretation of geophysical data at EL Fayoum-Dahshour Area, Egypt using 3-D models. *Arab J Sci Eng* 38:1769–1784
- Abdel Zaher M, Saibi H, Mansour K, Khalil A, Soliman M (2018) Geothermal exploration using airborne gravity and magnetic data at Siwa Oasis Western Desert, Egypt. *Renew Sustain Energy Rev* 82(3):3824–3832
- Abou Elenean KM (1997) Seismotectonics of Egypt in relation to the Mediterranean and Red Seas tectonics. Ph. D. Thesis, Ain Shams University, Egypt
- Abou Elenean KM, Mohamed AME, Hussein HM (2010) Source parameters and ground motion of the Suez-Cairo shear zone earthquakes, Eastern Desert, Egypt. *Nat Hazards* 52:431–451. <https://doi.org/10.1007/s11069-009-9388-x>
- Abu El-Ata AS, Abd El-Nabi SH (1985) Mapping the structural elements dissecting the CRETACEOUS rock units of the Qattara depressions area, western Desert, Egypt; using 3-D gravity modeling. *Geological survey of Egypt*. In: *Proc of 4th Ann.*, pp 103–23
- Afife M, Littke R, Lashin A, All MA (2018) Petrophysical reservoir-rock properties and source-rock characterization of Abu Roash Formation in Wadi El-Rayan oil field, Western Desert, Egypt. *Arab J Geosci* 11(14):378. <https://doi.org/10.1007/s12517-018-3694-0>
- Araffa SA, Monteiro Santos FA, Arafa-Hamed T (2012) Delineating active faults by using integrated geophysical data at northeastern part of Cairo, Egypt. *NRIAG J Astron Geophys* 1(1):33–44. <https://doi.org/10.1016/j.nrjag.2012.11.004>
- Araffa SA, Monteiro Santos FA, Arafa-Hamed T (2014) Assessment of subsurface structural elements around greater Cairo by using integrated geophysical tools. *Environ Earth Sci* 71:3293–3305. <https://doi.org/10.1007/s12665-013-2716-1>
- Ayyad MH, Darwish M (1996) Syrian arc structures: a unifying model of inverted basins and hydrocarbon occurrences in North Egypt.

- In: Proc. 13th petroleum exploration and production conference, vol 1. Egyptian Petroleum Corporation, Cairo, Egypt, pp 40–59
- Becken M, Burkhardt H (2004) An ellipticity criterion in magnetotelluric tensor analysis. *Geophys J Int* 159:69–82
- Booker J (2014) The magnetotelluric phase tensor: a critical review. *Surv Geophys* 35:7–40
- Bosworth W, El-Hawat AA, Helgeson DE, Burke K (2008) Cyrenaican “shock absorber” and associated inversion strain shadow in the collision zone of northeast Africa. *Geology* 36:695–698. <https://doi.org/10.1130/G24909A.1>
- Bown TM, Kraus M (1988) Geology and paleoenvironment of the Oligocene Jebel Qatrani Formation and adjacent rocks, Fayium Depression, Egypt. U.S. Geological Survey Professional Paper 1452
- Brimichi L, Khalil A, Kord'ik P, Mekkawi M, El-Bohoty M, Refai MK, Abdel Kader AK (2011) Active subsurface structures at Fayoum-Cairo district, Northern Western Desert, Egypt, as deduced from magnetic data. *Contrib Geophys Geod* 41/4:329–351
- Caldwell TG, Bibby HM, Brown C (2004) The magnetotelluric phase tensor. *Geophys J Int* 158(2):457–469
- Celebi TM, Sharp RV (1993) The October 12, 1992, Dahshur, Egypt, Earthquake. *Earthq Volcanoes (USGS)* 24(1):27–41
- Chave AD, Jones AG (2012) *The magnetotelluric method*. Cambridge University Press, Cambridge. <https://doi.org/10.1017/CBO9781139020138>
- Comeau MJ, Becken M, Käüfl JS et al (2020) Evidence for terrane boundaries and suture zones across Southern Mongolia detected with a 2-D magnetotelluric transect. *Earth Planets Space* 72:5. <https://doi.org/10.1186/s40623-020-1131-6>
- Di Paolo F, Ledo J, Ślęzak K et al (2020) La Palma Island (Spain) geothermal system revealed by 3D magnetotelluric data inversion. *Sci Rep* 10:18181. <https://doi.org/10.1038/s41598-020-75001-z>
- Egyptian General Petroleum Company (EGPC) (1987) Geological map of Egypt. NH 36 SW Beni Suef, Conoco Coral. Scale: 1:500000
- Fairhead JD, Watts AB, Chevalier P, El-Haddadeh B, Green CM, Stuart GW, Whaler KA, Whindle I (1988) African gravity project. Technical Report. University of Leeds Industrial Services Ltd., Leeds, United Kingdom
- Getech (1992) The African Magnetic Mapping Project. Commercial report (unpublished).
- Ghosh GK (2016) Interpretation of gravity data using 3D Euler deconvolution, tilt angle, horizontal tilt angle and source edge approximation of the north-west Himalaya. *Acta Geophys* 64(4):1112–1138. <https://doi.org/10.1515/acgeo-2016-0042>
- Green CM, Barritt SD, Fairhead JD, Misener DJ (1992) The African Magnetic Mapping Project. Extended Abstract, European Association of Geoscientists & Engineers (EAGE) 54th Meet Technical Exhibition: Paris
- Hammad MM, Awad SA, El Nady MM, Moussa DA (2010) The subsurface geology and source rocks characteristics of some jurassic and cretaceous sequences in the West Qarun Area, North Western Desert, Egypt. *Energy Sources Part a: Recovery Util Environ Effects* 32(20):1885–1898. <https://doi.org/10.1080/15567030701715955>
- Hersir G, Árnason K, Vilhjálmsson A, Saemundsson K, Ágústsdóttir Þ, Friðleifsson G (2020) Krýsuvík high temperature geothermal area in SW Iceland: geological setting and 3D inversion of magnetotelluric (MT) resistivity data. *J Volcanol Geotherm Res* 391:106500. <https://doi.org/10.1016/j.jvolgeores.2018.11.021>
- Hinze W, von Frese R, Saad A (2010) Gravity and magnetic exploration: principles, practices, and applications, pp 1–512. <https://doi.org/10.1017/CBO9780511843129>.
- Käüfl JS, Grayver AV, Comeau MJ, Kuvshinov AV, Becken M, Kamm J, Batmagnai E, Demberel S (2020) Magnetotelluric multiscale 3-D inversion reveals crustal and upper mantle structure beneath the Hangai and Gobi-Altai region in Mongolia. *Geophys J Int* 221(2):1002–1028. <https://doi.org/10.1093/gji/ggaa039>
- Key K (2016) MARE2DEM: a 2-D inversion code for controlled-source electromagnetic and magnetotelluric data. *Geophys J Int* 207(1):571–588. <https://doi.org/10.1093/gji/ggw290>
- Khalil MH, Moustafa AR (1994) Tectonic framework of Northeast Egypt and its bearing hydrocarbon exploration. In: Proc. 12th petroleum exploration and production conference, vol 1. Egyptian Petroleum Corporation, Cairo, pp 67–86
- Khalil A, Toni M, Hassoup A, Mansour K (2014) Analysis of aeromagnetic data for interpretation of seismicity at Fayoum-Cairo area, Egypt. *Earth Sci Res J* 18(1):7–13
- Kirkby AL, Zhang F, Peacock J, Hassan R, Duan J (2019) The MTPy software package for magnetotelluric data analysis and visualisation. *J Open Source Softw* 4(37):1358. <https://doi.org/10.21105/joss.01358>
- Krieger L, Peacock J (2014) MTPy: a python toolbox for magnetotellurics. *Comput Geosci* 72:167–175. <https://doi.org/10.1016/j.cageo.2014.07.013>
- Melo FF, Barbosa VCF (2018) Correct structural index in Euler deconvolution via base-level estimates. *Geophysics* 83:J87–J98. <https://doi.org/10.1190/geo2017-0774.1>
- Mossaad M (1996) Liquefaction during the October 12, 1992 Dahshour, Egypt, earthquake and its potential in The Nile valley and delta. *Soils Found* 36(2):13–27
- Moustafa AR (2010) Structural setting and tectonic evolution of north Sinai folds, Egypt. In: Homborg C, Bachmann M (eds) Evolution of the levant margin and Western Arabia platform since the Mesozoic, vol 341. *Geol. Soc. Lond. Spec Publ*, pp 37–63
- Moustafa SR, Takenaka H (2009) Stochastic ground motion simulation of the 12 October 1992 Dahshour earthquake. *Acta Geophys* 57(3):636–656
- Othman A, Fathy M, Ali AS (2016) Geophysical evaluation for Wadi Rayan Field, Western Desert, Egypt. *Egypt J Petroleum* 25:125–132
- Pirttijärvi M (2004) BLOXER. Interactive visualization and editing software for 3-D block models, version 1.5, user's guide, Geophysical survey of Finland, Report Q16.2/2004/1
- Reid AB, Thurston JB (2014) The structural index in gravity and magnetic interpretation: errors, uses, and abuses. *Geophysics* 79(4):J61–J66
- Said R (1981) *The geological evolution of the River Nile*. Elsevier Publ. Co., Amsterdam, p 180
- Simpson F, Bahr K (2005) *Practical magnetotellurics*. Cambridge University Press, Cambridge, 272 p. <https://doi.org/10.1017/CBO9780511614095>
- Thompson DT (1982) EULDPH. A new technique for making computer assisted depth estimates from magnetic data. *Geophysics* 47:31–37
- Tracy A, Javernick-Will A (2020) Credible sources of information regarding induced seismicity. *Sustainability* 12(6):2308. <https://doi.org/10.3390/su12062308>